Spacecraft Re-Entry Impact Point Targeting using Aerodynamic Drag

Sanny R. Omar[1] and Riccardo Bevilacqua[2]
University of Florida, ADAMUS Laboratory, Gainesville, FL 32611

The ability to re-enter the atmosphere at a desired location is important for spacecraft containing components that may survive re-entry. While impact point targeting has traditionally been initiated through impulsive burns with chemical thrusters on large vehicles such as the Space Shuttle, and the Soyuz and Apollo capsules, many small spacecraft do not host thrusters and require an alternative means of impact point targeting to ensure that falling debris do not cause harm to persons or property. This paper discusses the use of solely aerodynamic drag force to perform this targeting. It is shown that by deploying and retracting a drag device to vary the ballistic coefficient of the spacecraft, any desired longitude and latitude on the ground can be targeted provided that the maneuvering begins early enough and the latitude is less than the inclination of the orbit. An analytical solution based on perturbations from a numerically propagated trajectory is developed to map the initial state and ballistic coefficient profile of a spacecraft to its impact point. This allows the ballistic coefficient profile necessary to reach a given target point to be rapidly calculated, making it feasible to generate the guidance for the decay trajectory onboard the spacecraft. The ability to target an impact point using aerodynamic drag will enhance the capabilities of small spacecraft and will enable larger space vehicles containing thrusters to save fuel by more effectively leveraging the available aerodynamic drag.

Nomenclature

A	=	satellite area [m^2]
a	=	semi major axis [km]
a_d	=	acceleration due to aerodynamic drag [m/s^2]
ADAMUS	=	Advanced Autonomous Multiple Spacecraft (laboratory)
a_0	=	reference semi major axis for exponential atmospheric model [km]
a_i	=	initial semi major axis in maneuver [km]
a_f	=	final semi major axis in maneuver [km]
a_{swap}	=	semi major axis at which ballistic coefficient is changed [km]
C_b	=	ballistic coefficient [m^2/kg]
C_{b1}	=	ballistic coefficient from t_0 to t_{swap} in maneuver [m^2/kg]
C_{b2}	=	ballistic coefficient from t_{swap} until terminal point in maneuver [m^2/kg]
$C_{b_{avg}}$	=	average ballistic coefficient [m^2/kg]
C_d	=	drag coefficient [no units]
e	=	eccentricity [no units]
F_r	=	non-Keplerian acceleration in the radial direction [km/s^2]
F_s	=	non-Keplerian acceleration in the along-track direction [km/s^2]
H	=	atmosphere scale height [km]
i	=	orbit inclination [rad]
m	=	satellite mass [kg]
n	=	mean motion [rad/s]
p	=	semi latus rectum [km]

[1] PhD Student, Department of Mechanical and Aerospace Engineering, MAE-A Room 211, AIAA Student Member.
[2] Associate Professor, Department of Mechanical and Aerospace Engineering, MAE-A Room 308, AIAA Senior Member.

r = orbital radius [km]
$t_{deorbit}$ = time at which the satellite deorbits [s]
t_{step} = time increment between tested t_{swap} values [s]
t_{swap} = time at which the ballistic coefficient is changed from C_{b1} to C_{b2} [s]
t_{swap_ref} = swap time in the reference trajectory [s]
t_{term} = time at which the satellite enters the terminal phase of its trajectory [s]
v = orbital velocity [km/s]
$\Delta\theta_{10}$ = change in true anomaly from t_0 until t_{swap} in the initial trajectory [rad]
$\Delta\theta_{20}$ = change in true anomaly from t_{swap} until t_{term} in the initial trajectory [rad]
$\Delta\theta_1$ = change in true anomaly from t_0 until t_{swap} in the new trajectory [rad]
$\Delta\theta_2$ = change in true anomaly from t_{swap} until t_{term} in the new trajectory [rad]
$\Delta\theta_t$ = desired total change in true anomaly of new trajectory until the terminal point [rad]
$\Delta\theta_d$ = difference in total change in true anomaly between the new trajectory and the initial trajectory [rad]
Δt_{10} = time until swap point (equivalent to t_{swap}) in initial trajectory [s]
Δt_{20} = time from the swap point until terminal point in the initial trajectory [s]
Δt_1 = time until swap point (measured from simulation epoch) in the new trajectory [s]
Δt_2 = time from swap point until the terminal point in the new trajectory [s]
Δt_t = total time the new trajectory takes to reach the terminal point [s]
Δt_d = difference in total orbit lifetime between the new trajectory and the initial trajectory [s]
ΔC_b = term used to correlate C_{b1} and C_{b2} [no units]
θ = true anomaly [rad]
μ = Earth's gravitational parameter [km^3/s^2]
ρ = ambient density [kg/m^3]
ρ_0 = density at reference altitude (a_0 – earth radius) [kg/m^3]
Ω = right ascension of the ascending node [rad]
ω = angular velocity [rad/s], argument of the periapsis [rad]

I. Introduction

ENSURING that space vehicles cause no damage to persons or property after de-orbit has been an important consideration since the beginning of the space program[1,2]. Most large space vehicles containing thrusters execute a precise de-orbit burn to initiate the re-entry trajectory[3]. Because the time required for this burn is generally short compared to the duration of the decay trajectory, it can be treated as a nearly instantaneous impulse (impulsive burn), making it relatively easy to calculate the burn's effects on the spacecraft's decay trajectory. Additionally, because de-orbit generally occurs within one or two orbits after the de-orbit burn, the re-entry guidance can be computed on the ground and uplinked to the spacecraft, leaving the spacecraft navigation and control system responsible only for tracking the precomputed guidance (usually through variation of the spacecraft's lift to drag ratio)[4,5]. In recent years, the miniaturization of technology has brought about small spacecraft such as CubeSats[6] that may not contain thrusters or attitude control systems, and generally do not perform active re-entry control. These satellites have generally been built by universities[7] and small organizations as teaching tools or testbeds for low-cost scientific experiments or technology demonstrations. As such, benign materials are generally used, and most components of the spacecraft are destroyed during re-entry and pose no threat to ground assets. However, there currently is an increasing demand for small satellites capable of performing advanced missions including Earth imaging, commercial communications, and astronomical observations. Performing these missions sometimes requires heavy metals or other materials that do not vaporize on re-entry[1] which may cause a hazard to people on the ground. Satellites containing such materials may not be allowed to launch unless they have a means of guaranteeing safe and controlled re-entry.

If a propulsion system is not an option (due to cost or volume constraints), changing the aerodynamic drag the spacecraft experiences through modulation of the ballistic coefficient presents itself as the most feasible way to perform re-entry targeting. While extensive work has been done on density modeling and spacecraft drag estimation[8,9], and there is a body of research focused on relative spacecraft maneuvering using differential drag[10–12], very little research has been conducted on a de-orbit algorithm that utilizes solely aerodynamic drag to control the decay trajectory. Though the modulation of vehicle aerodynamics has been utilized since the Apollo missions[4] to help vehicles maintain a precomputed guidance during the re-entry trajectory, the use of solely aerodynamic drag for re-entry targeting presents a much greater challenge and has never been done before to the best of the authors' knowledge. This is likely because the procedure is difficult, requires computing power beyond what was available on legacy space

vehicles, and because until recently, there has not been a significant class of thruster-less spacecraft demanding such an algorithm. Because drag force is small and only acts in the retrograde direction, maneuvering must begin several days before expected re-entry. If maneuvering is not initiated early enough, it may not be possible to target the desired longitude and latitude as will be demonstrated in the section IV (Controllability Analysis). Additionally, uncertainties in atmospheric density and spacecraft ballistic coefficients will significantly impact the decay trajectory because the errors propagate for multiple days. This and the inability to control out of plane motion using aerodynamic drag mean that a periodic re-computation of the guidance trajectory onboard the spacecraft will likely be required.

The most recent targeted de-orbit algorithm is published in Ref. 13, and is based on a two-phase decay trajectory. During the first phase, the satellite maintains a ballistic coefficient of C_{b1} until some semi major axis a_{swap} is reached. After this point (phase 2), the satellite maintains a ballistic coefficient of C_{b2}. This algorithm utilizes an analytical solution to create a mapping from the initial conditions and control parameters (C_{b1}, C_{b2}, and a_{swap}) to the re-entry point. The mapping is then utilized to analytically calculate the control parameters needed to target a desired location. The analytical solution, however, presents some limitations. For one, the analytical solution requires an exponential atmospheric model with density given as

$$\rho = \rho_0 \exp\left[-\frac{a - a_0}{H}\right] \tag{1}$$

If the orbit is assumed circular, the total time and change in true anomaly that occur as a satellite under the influence of aerodynamic drag decays from one semi major axis to another is given by the equations

$$\Delta t = \int_{a_0}^{a_f} -\frac{da}{2\sqrt{\mu a} C_b \rho} \tag{2}$$

$$\Delta\theta = \int_{a_0}^{a_f} \frac{da}{2C_b a^2 \rho} \tag{3}$$

Equations (2) and (3) are then integrated analytically after substituting Eq. (1) for ρ. This yields

$$\Delta t = \frac{\sqrt{\pi H}}{-2C_b\sqrt{\mu}\rho_0 e^{\frac{a_0}{H}}}\left[erfi\left(\sqrt{\frac{a_f}{H}}\right) - erfi\left(\sqrt{\frac{a_i}{H}}\right)\right] \tag{4}$$

$$\Delta\theta = \frac{-1}{-2C_b\rho_0 H e^{\frac{a_0}{H}}}\left[\frac{a_f Ei\left(a_f/H\right) - He^{a_f/H}}{a_f} - \frac{a_i Ei(a_i/H) - He^{a_i/H}}{a_i}\right] \tag{5}$$

where *erfi* and *Ei* are the imaginary error function and exponential integral respectively. The changes in time and true anomaly during phases one and two can be combined to calculate the total orbit lifetime and total change in true anomaly which can be used to calculate the impact location. This approach presents several issues. First of all, the exponential integral and imaginary error function become large within the range of possible input values, leading to significant truncation errors during practical computations. The algorithm also cannot be employed if the atmospheric model is not exponential, because there would be no closed form solution to the integrals in Eq. (1) and Eq. (2). A non-exponential density profile could be broken into bands where the density in each band increases roughly exponentially, but this still introduces some error. In addition, the errors resulting from the circular orbit assumption grow over time, causing significant error. Finally, the algorithm only calculates the time and true anomaly change to get to the atmospheric interface (about 150 km), not all the way to the ground. This is because the orbit ceases to remain circular below this point and the assumptions used to derive Eq. (1) and Eq. (2) no longer hold.

To simplify the process of calculating the control parameters needed for re-entry targeting, the authors of Ref. 13 define ΔC_b such that

$$C_{b1} = C_{b_{avg}}(1 + \Delta C_b) \tag{6}$$

$$C_{b2} = C_{b_{avg}}(1 - \Delta C_b) \tag{7}$$

ΔC_b and a_{swap} now become the control parameters utilized for targeting. Once these parameters are estimated using the analytical solution, they are sent to a numerical optimizer. Unfortunately, this problem has numerous combinations of control parameters that act as local minimizers of the error between the desired and actual re-entry locations as seen in Figure 2. Thus, especially since the error in the analytical solution may be large, there is no guarantee that the numerical optimization scheme will converge to the control parameters that globally minimize the targeting error. Additionally, while using the semi major axis as the condition for switching the ballistic coefficient may work in the simulator, the semi major axis will oscillate in reality due to the non-uniform gravitational field of the Earth and other environmental perturbations such as solar gravity, lunar gravity, and solar radiation pressure. This is the case even if mean orbital elements are used as shown in Figure 1. Figure 2 illustrates the targeting error that results with various

control parameter values for an initial 300 km circular orbit with $C_{b_{avg}} = .0343\frac{m^2}{kg}$. Note that t_{swap} is utilized instead of a_{swap} to mark the point where the ballistic coefficient transitions from C_{b1} to C_{b2}.

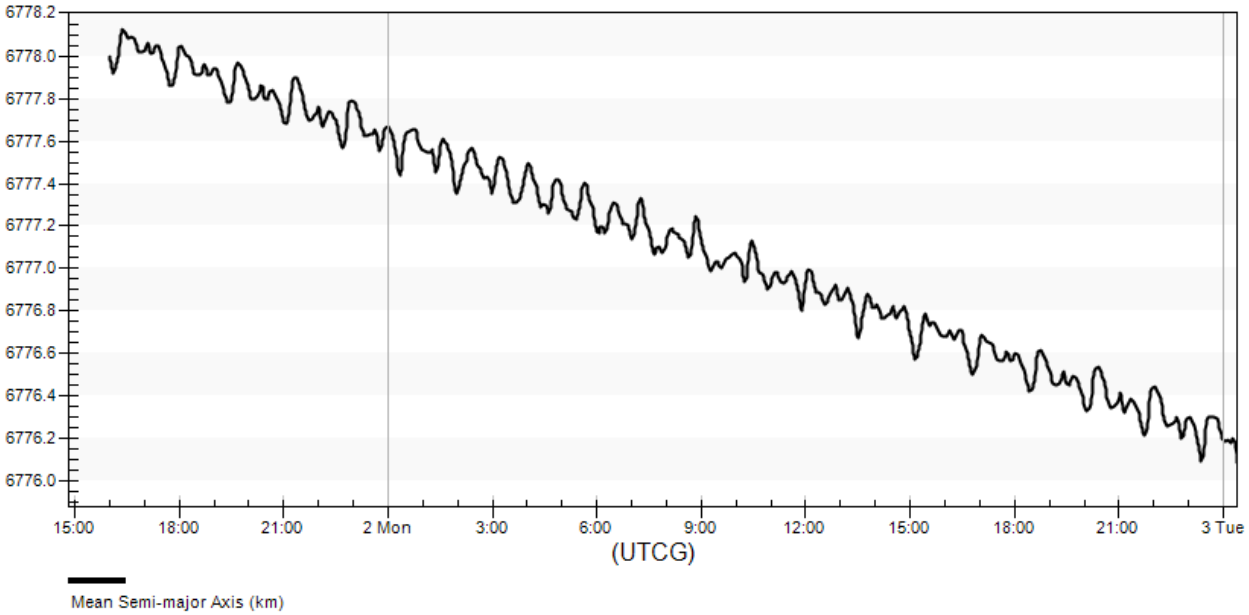

Figure 1 . Oscillations in Mean Semi Major Axis over Time Due to Environmental Perturbations[14]

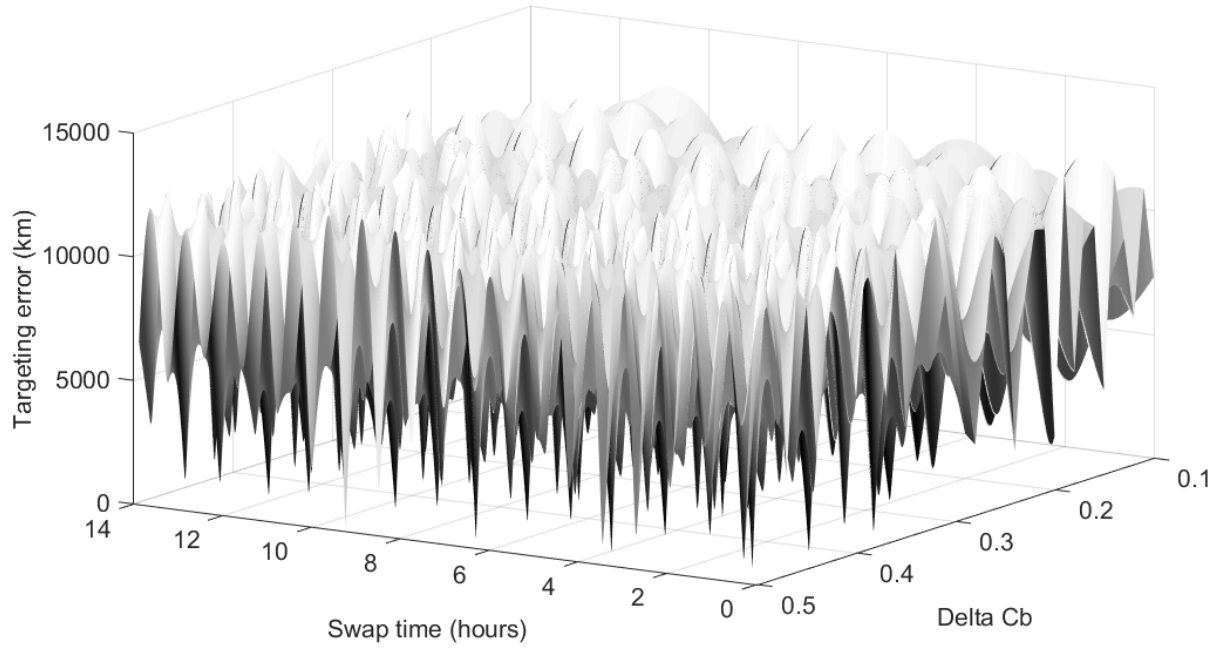

Figure 2. Targeting Error for Various Combinations of Swap Time and Delta C_b (note: ΔC_b is adimensional (equations (6) and (7))).

Despite these challenges, the increasing power of modern computers and the development of a drag device by the University of Florida ADAMUS laboratory make targeted de-orbit using solely aerodynamic drag feasible[15,16]. This paper discusses an algorithm by which the ballistic coefficient of a spacecraft can be varied to achieve a desired spacecraft re-entry location. Increasing the ballistic coefficient reduces orbit lifetime while decreasing the ballistic coefficient increases lifetime. The ability to modulate the ballistic coefficient at will enable the definition of a ballistic coefficient profile that causes the spacecraft to re-enter in a desired location. With this re-entry control scheme, small spacecraft equipped with the drag device can safely re-enter away from populated areas. This control scheme could

also enable spacecraft to fly through particular regions of the atmosphere during the decay trajectory if the satellite operators wished to conduct scientific observations in that region. Satellites or re-entry vehicles containing thrusters could also utilize this control scheme (provided that they have a means of varying their ballistic coefficient) in order to conserve fuel during re-entry.

The algorithm proposed in this paper results offers improvements over the algorithm in Ref. 13. The new algorithm likewise divides the decay trajectory into two phases and analytically maps initial conditions and control parameters to impact location. In this case, the control parameters will be C_{b1}, C_{b2}, and t_{swap}. However, instead of relying on the assumption of a perfectly circular orbit and an exponential atmosphere, this analytical solution is based on perturbations from a numerically propagated trajectory. To generate this initial trajectory, the spacecraft orbit is propagated from its initial conditions with some C_{b1}, C_{b2}, and t_{swap}. For small changes in the control parameters where the density encountered at each altitude does not change much and the velocity profile of the spacecraft remains roughly the same, an analytical solution can be utilized to predict where a spacecraft will land based on the initial trajectory without having to propagate another entire trajectory. This makes characterization of the perturbed trajectory almost instantaneous, simplifying the calculation of the control parameters needed to target a ground point. Additionally, because the initial trajectory is numerically propagated, any atmospheric model can be used (including advanced models such as NRLMSISE and JB2008) and effects such as Earth's oblateness can also be added. Furthermore, the effects of noncircular orbits, variations in density, and environmental perturbations such as solar and lunar gravity are captured in the propagation of the reference trajectory, so the errors in the analytical solutions are small as long as perturbations in the control parameters are small. Section II discussed the analytical mapping from the initial state and control parameters to impact location. Section III discusses a means of using this mapping to analytically determine a set of control parameters that sufficiently minimize latitude and longitude targeting error. A new initial trajectory can then be formulated with the original initial orbital conditions and the newly calculated control parameters. The impact point resulting after numerical propagation of this new trajectory will be close to the analytically predicted impact point, the perturbation in control parameters will be smaller than in the first iteration, and the discrepancy between the numerical and analytical solutions will be smaller. With each iteration, smaller and smaller perturbations from the reference trajectory are needed so the analytical solution errors become even smaller. After only a few iterations, the numerical and analytical solutions converge and the control parameters needed for impact point targeting are calculated. Because this approach requires only a few numerical propagations, the run time of the algorithm is generally under five minutes using MATLAB R2016a on a modern laptop with a 2.4 GHz processor. This makes the targeting algorithm feasible to run onboard a spacecraft with limited computational power, especially if additional code optimization is performed and the code is re-written in a faster language such as C. Simulation results and performances are discussed in detail in Section V. Additionally, the analytical solutions allow for a detailed view of the effects of changing certain control parameters on the impact location. This facilitates a controllability analysis which is discussed in Section IV.

II. Analytical Mapping from Initial State to Impact Location

The first step in this algorithm is to propagate an initial trajectory. Based on this initial trajectory, the impact location of a satellite with the same initial conditions but a different ballistic coefficient profile can be calculated analytically.

A. Analyzing Effects of Orbital Perturbations

In order to use analytical techniques to calculate impact location, we need to develop some relations between the changes in the orbital elements and the aerodynamic drag force. Assuming that the orbit is roughly circular facilitates the development of these relations. The Gaussian Variation of Parameters equations from Eq. 9-24 in Ref. [17] give the change in semi major axis over time as

$$\frac{da}{dt} = \frac{2}{n\sqrt{1-e^2}}\left[e \sin\theta \, F_R + \frac{p}{r} F_s\right] \tag{8}$$

For a circular orbit $e = 0$, $p = r$, and $F_s = a_d$ and so Eq. (8) simplifies to

$$\frac{da}{dt} = \frac{2a_d}{n} \tag{9}$$

Mean motion (n) is the average angular velocity of a spacecraft in orbit. For a circular orbit, instantaneous angular velocity is equal to mean motion. Mean motion is given by the equation

$$n = \sqrt{\frac{\mu}{a^3}} \tag{10}$$

Acceleration due to drag is given by the equation

$$a_d = -C_b \rho v^2 \tag{11}$$

Where

$$C_b = \frac{C_d A}{2m} \tag{12}$$

Substituting Eqs. (10)-(12) into Eq. (9) and rearranging yields

$$-\sqrt{\frac{\mu}{a^3}}\left(\frac{1}{2C_b \rho v^2}\right) da = dt \tag{13}$$

The velocity in a circular orbit is given by

$$v = \sqrt{\frac{\mu}{a}} \tag{14}$$

Substituting Eq. (14) for *v* in Eq. (13) yields

$$-\frac{da}{2\sqrt{\mu a} C_b \rho} = dt \tag{15}$$

The time required for a spacecraft in a circular orbit to fall from an initial semi major axis (a_0) to a final a_f can be calculated by integrating Eq. (15)

$$\Delta t = \int_{a_0}^{a_f} -\frac{da}{2\sqrt{\mu a} C_b \rho} \tag{16}$$

C_b is a constant and can be factored out of the integral.

$$\Delta t C_b = \int_{a_0}^{a_f} -\frac{da}{2\sqrt{\mu a} \rho} \tag{17}$$

If we assume that the density is a function of only altitude, then the density will also be a function of semi major axis for a circular orbit. With this assumption, *a* is the only variable in the integral in Eq. (17). Thus, when evaluated, the solution to the integral will be a function of *a* (call it *G(a)*). Eq. (17) becomes

$$\Delta t C_b = G(a_f) - G(a_0) \tag{18}$$

This relation shows that the time required to drop from a_0 to a_f varies linearly with the ballistic coefficient. For example, if the ballistic coefficient is doubled, the time required is cut in half. If the time required for a satellite with C_{b1} to go from a_0 to a_f is t_1, then the time (t_2) required for a satellite with C_{b2} to achieve the same change in semi major axis can be written as

$$t_2 = \frac{C_{b1} t_1}{C_{b2}} \tag{19}$$

Additionally, for a circular orbit, mean motion is the time rate of change or true anomaly (θ) given by

$$n = \frac{d\theta}{dt} \tag{20}$$

Multiplying Eq. (20) by Eq. (15) yields

$$\frac{d\theta}{da} = -\frac{n}{2\sqrt{\mu a} C_b \rho} \tag{21}$$

Substituting Eq. (10) for *n* in Eq. (21) yields

$$\frac{d\theta}{da} = -\frac{1}{2a^2 C_b \rho} \tag{22}$$

Multiplying both sides of Eq. (22) by $C_b(da)$ (ballistic coefficient times differential change in semi major axis) and integrating yields

$$(\Delta\theta) C_b = \int_{a_0}^{a_f} \frac{da}{2a^2 \rho} \tag{23}$$

Once again, if density is a function of *a*, the integral in Eq. (23) will also be a function of *a* when evaluated. If we call this function *P(a)*, the Eq. (23) becomes

$$(\Delta\theta) C_b = P(a_f) - P(a_0) \tag{24}$$

This shows that the change in true anomaly as a satellite falls from a_0 to a_f varies linearly with C_b. The average angular velocity of the spacecraft from a_0 to a_f can be calculated by dividing Eq. (24) by Eq. (18).

$$\omega_{avg} = \frac{\Delta\theta}{\Delta t} = \frac{P(a_f) - P(a_0)}{G(a_f) - G(a_0)} \tag{25}$$

Note that in Eq. (25), C_b simplifies and ω_{avg} is a function of only the initial and final semi major axes. This proves that the average angular velocity of a spacecraft from a_0 to a_f is independent of spacecraft ballistic coefficient assuming that the orbit is circular and that density is a function of *a* only.

B. Issues with This Procedure

In reality, even orbits that begin circular will not remain perfectly circular when under the influence of aerodynamic drag, even if there are no other perturbations. Both the altitude and velocity will oscillate slightly, especially as the orbit decays and the drag force becomes stronger as shown in Figure 3. This is because for any starting point in an initially circular orbit, the aerodynamic drag force will slightly reduce the instantaneous velocity at that point and make it the orbit apogee. The altitude at the orbit's new perigee will then be lower, the density higher, and the velocity greater than at the apogee, so the drag force will be greater. This will cause what was formerly the perigee to become the apogee. This cycle continuous until de-orbit causing the oscillations in velocity and altitude seen in Figure 3.

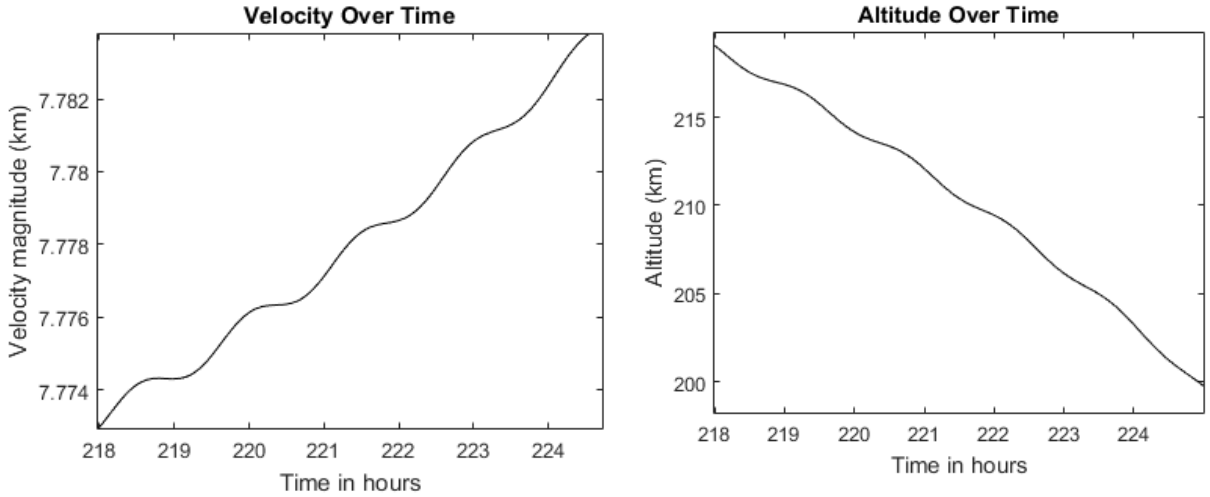

Figure 3.Velocity and Altitude over Time during Decay Trajectory

Though these oscillations are small, they mean that the velocity, density, and drag profiles will be slightly different than expected for a circular orbit and the use of Equations (19) and (25) will introduce small errors that can accumulate over time. Additionally, the density is not, in reality, a function of only semi major axis and can vary widely at any given altitude based on solar and geomagnetic activity as seen in Figure 4.

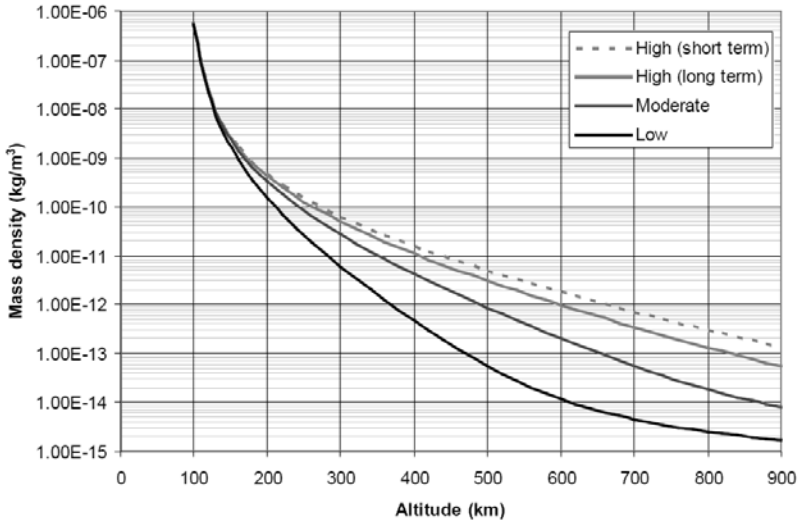

Figure 4. JB2008 Mean Air Density vs. Altitude Based on Solar and Geomagnetic Activity[18]

All these factors introduce errors, but since the targeting algorithm is based on perturbations from a numerically propagated trajectory, the drag force fluctuations and deviations from the circular orbit will be captured in the numerical trajectory. This minimizes error and makes the relations in Eqs. (19), (24), and (25) usable in the targeting algorithm which calculates the control parameters (ballistic coefficient profile) needed for the spacecraft to impact a desired longitude and latitude.

C. Calculating Impact Location Based on Applied Controls

The targeting algorithm requires the ability to calculate where a satellite will land given a set of initial conditions and applied controls (C_{b1}, C_{b2}, and t_{swap}). This can be performed by first propagating an initial trajectory and analyzing perturbations from this initial trajectory. Having an analytical relation mapping the initial conditions and applied controls to the final impact location facilitates the rapid testing of numerous combinations of control parameters until the optimal set of controls is found. This analytical mapping is defined based on a single numerically propagated reference trajectory is as follows:

1. The initial trajectory is propagated from the initial conditions with a chosen C_{b10} until time t_{swap_ref}. After this time, the ballistic coefficient becomes C_{b20}, and the trajectory is propagated until a specified final semi major axis is reached. This is considered the terminal point of the trajectory and occurs at time t_{term}. Below the terminal point, wide variations in the drag coefficient may occur and the circular orbit assumptions are no longer valid. After t_{term}, the satellite takes on a ballistic coefficient C_{b3} and the trajectory is propagated until ground impact. When generating new trajectories, it is assumed that the ballistic coefficient during the terminal phase of the new trajectory is the same as during the terminal phase of the initial trajectory. For this reason, the terminal phase can be characterized by an amount of time ($t_{deorbit}$ - t_{term}) and a change in true anomaly ($\Delta\theta_{term}$) between the terminal point and the impact point. For each new set of control parameters, the new location of the terminal point is determined and $\Delta\theta_{term}$ is added to the true anomaly at this point to determine the new impact point location. Because $\Delta\theta_{term}$ and ($t_{deorbit}$ - t_{term}) remain the same for any new trajectory and the inclination of the orbital plane is known, the location of the terminal point required to target the desired latitude and longitude impact point can be uniquely determined. The goal of the targeting algorithm is now to define a new trajectory that passes through the terminal point, as this will guarantee that the spacecraft impacts the desired longitude and latitude on the ground.
    1.1. During propagation of the initial trajectory, the time, position, and velocity at each time step are recorded
    1.2. The average angular velocity from t_0 to the current time (t) and from t to t_{term} are also recorded at each time step
2. Equations (19) and (25) are used to determine the terminal point location of a spacecraft with the same initial conditions and different C_{b1}, C_{b2}, and t_{swap}. The analysis is done by breaking the new trajectory into three phases. Each phase is represented by an initial and final semi major axis (a_i and a_f) such that the spacecraft in the new trajectory and the initial trajectory do not change their ballistic coefficients between a_i and a_f. This enables the analysis of the behavior (change in orbital elements over time) of the new trajectory in each phase based on the behavior of the reference trajectory in the corresponding phase (a_i to a_f).
    2.1. Since the time and ballistic coefficient for each phase of the initial trajectory are known and the ballistic coefficient in the new trajectory in the corresponding phase is known, Eq. (19) can be utilized to calculate the time required to complete each phase of the new trajectory.
    2.2. From Eq. (25), we known that the average angular velocity in each phase of the new trajectory is the same as the average angular velocity of the reference trajectory in the corresponding phase because both phases have the same a_i and a_f.
    2.3. Since the time and average angular velocity in each phase of the new trajectory are known, the total change in true anomaly in each phase can be found my multiplying the time by the average angular velocity.
    2.4. The total orbit lifetime of the new trajectory until the terminal point can be found by adding the times required for each phase. Similarly, the total change in true anomaly until the terminal point can be found by adding the changes in true anomaly that occur during each phase.
    2.5. Assuming that the true anomaly and semi major axis are the only orbital elements that are changing and $\Delta\theta_{term}$ and ($t_{deorbit}$ - t_{term}) remain constant for any new trajectory, the time and orbital elements of the spacecraft at de-orbit can be calculated. These orbital elements can be converted to the ECI frame and can then be converted (using impact time) to impact latitude and longitude. Because we only care about impact location, the orbital elements at the terminal point with $\Delta\theta_{term}$ added to the true anomaly and ($t_{deorbit}$ - t_{term}) added to the time can be used as the impact point orbital elements for the purpose of calculating impact latitude and longitude.
    2.6. We now have a mapping from initial conditions and control parameters to impact location. Figure 5 illustrates the partitioning of the new and reference trajectories into phases for the case where t_{equiv} is less than t_{s_old}. The phases are bounded by the time points t_0, t_{s_new}, t_{s_old}, t_{eq_en}, t_{equiv}, t_{f_old}, and t_{f_new} defined as follows:
        2.6.1. t_0: Initial time
        2.6.2. t_{s_new}: New swap time
        2.6.3. t_{s_old}: Swap time in initial trajectory

2.6.4. t_{eq_en}: Point in new trajectory where the energy of the orbit (and semi major axis) is the same as the energy of the initial trajectory at time t_{s_old}

2.6.5. t_{equiv}: Time in the initial trajectory at which the energy of the orbit is the same as the energy of the new trajectory at t_{s_new}

2.6.6. t_{f_old}: Time until the terminal point in the initial trajectory

2.6.7. t_{f_new}: Time until the terminal point in the new trajectory

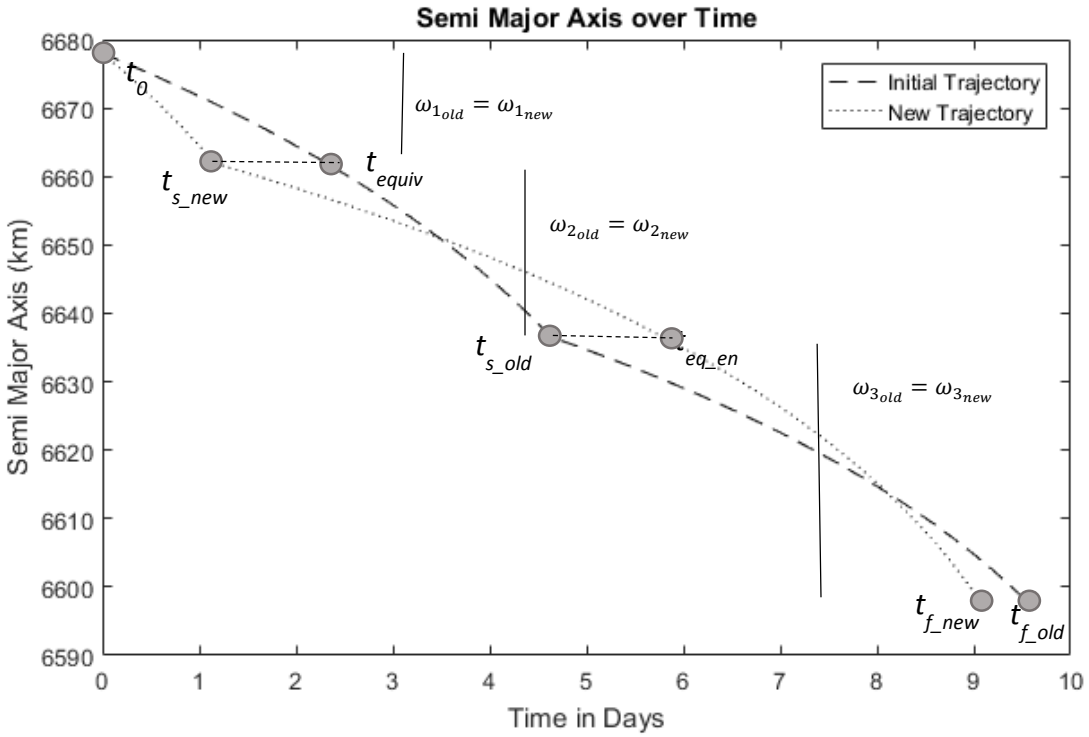

Figure 5. Semi Major Axis over Time for Old and New Trajectories

Now that an analytical relationship has been developed relating the initial state and control parameters (C_{b1}, C_{b2}, and t_{swap}) to the final impact location, the effects of variations in the control parameters on impact location can be more easily analyzed. Note that if J2 effects are included in the simulation, the analytical mapping must take into account the rate of precession of the orbital plane caused by J2 when calculating the impact location.

III. Latitude and Longitude Targeting Algorithm

Using the analytical relationship between the control parameters and impact location developed in Section II, the tasks of latitude and longitude targeting can be decoupled. Latitude targeting will be addressed first. Assuming that C_{b1} and C_{b2} have different values and maneuvering is initiated with sufficient time (quantified later) before de-orbit, it will be possible to target any latitude below the orbit inclination by varying only t_{swap}. The simplest and most reliable way to perform this latitude targeting is to define a range of acceptable t_{swap} values (discussed in Section IV. Controllability Analysis) and test the impact location resulting from all t_{swap} values within that range separated by a time increment t_{step}. The set of tested t_{swap} values will be

$$t_{swap} \in [t_{s\_min}, t_{s\_min} + t_{step}, t_{s\_min} + 2t_{step}, \dots, t_{s\_max}] \tag{26}$$

After each new tested t_{swap} value, the latitude and longitude errors are recorded. When the sign of the latitude error (actual – desired latitude) changes between two t_{swap} values (t_{s1} and t_{s2}), we know that a t_{swap} value that yields zero latitude error lies between t_{s1} and t_{s2} as illustrated in Figure 6. The bisection method can then be utilized to find this t_{swap} value. In general, there will be multiple possible t_{swap} values that yield zero latitude error. Out of these, the one that also results in the minimum positive longitude error should be chosen.

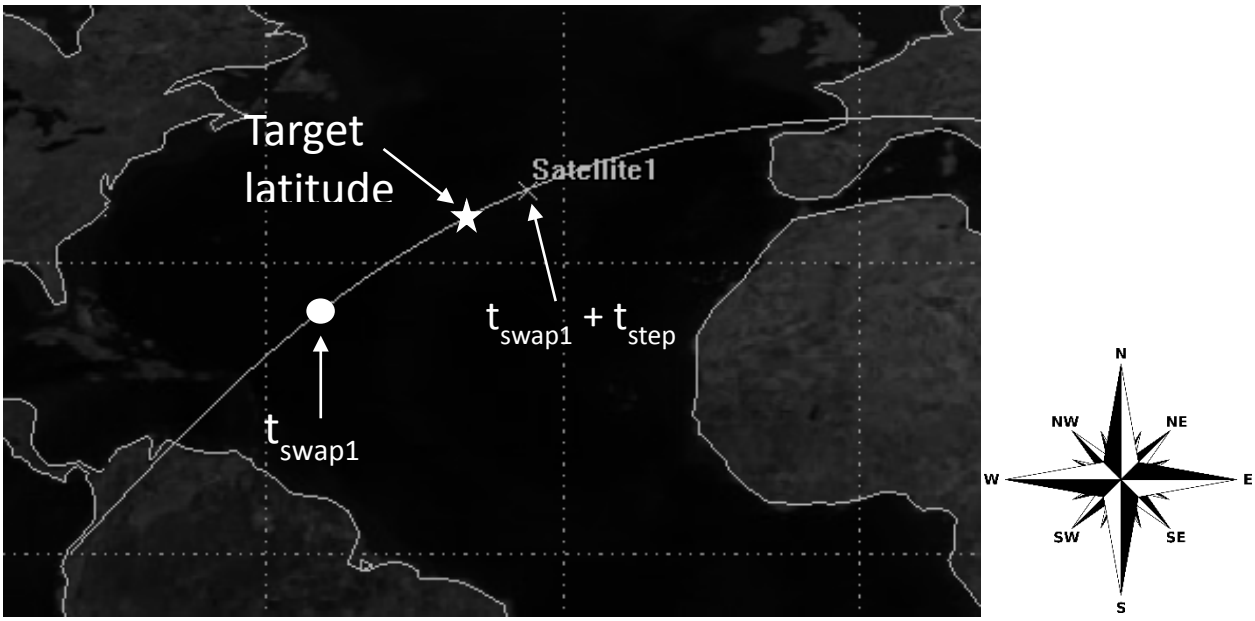

Figure 6. Using the Bisection Method for Latitude Targeting[14]

A positive longitude error (satellite east of impact point) means that the orbit would have to last slightly longer with the same total change in true anomaly to achieve the desired longitude targeting. A negative longitude error (satellite west of impact point) means the orbit would have to last shorter to achieve the desired longitude targeting. A positive longitude error is desirable because the initial control parameters will be configured to enhance the ability to increase orbit life at the cost of reducing the ability to decrease orbit life while maintaining a constant total change in true anomaly. This is discussed further in section IV (Controllability Analysis). Once the optimal t_{swap} value has been selected, the C_{b1} and C_{b2} values will be varied to eliminate the remaining longitude error without causing additional latitude error. This will be done by changing the total orbit lifetime without changing the total change in true anomaly. If the total change in true anomaly remains constant, the final impact latitude (and hence latitude error) will remain the same. The fact that the mean motion (average angular velocity) of the spacecraft at larger semi major axes is less than at lower semi major axes makes it possible to change the total orbit lifetime without varying the total change in true anomaly. An increase in orbit lifetime could be achieved by reducing C_{b1} while increasing C_{b2}. This would mean that the satellite spends more time at a greater semi major axis. Because this greater semi major axis means a slower mean motion, the satellite will orbit longer for the same total change in true anomaly. Conversely, to reduce the total orbit lifetime without varying the total change in true anomaly, C_{b1} would be increased while C_{b2} would be reduced. This would mean that the satellite spends more time in the lower orbit and experiences a greater average mean motion. Thus, the satellite would experience a shorter orbit lifetime for a given total change in true anomaly.

From the definitions of the variables ($t_{s_{old}}$, $t_{s_{new}}$, C_{b10}, C_{b20}, C_{b1}, C_{b2}, $\Delta\theta_{10}$, $\Delta\theta_{20}$, $\Delta\theta_1$, $\Delta\theta_2$, $\Delta\theta_t$, $\Delta\theta$, $\Delta t_{10}, \Delta t_{20}, \Delta t_1, \Delta t_2$, Δt_t, Δt) in the Nomenclature section and from Eqs. (19) and (24) , we can quantify the effects of changes in the ballistic coefficients on impact location. Assuming also that the drag configurations are swapped at the same semi major axis in the new and initial trajectories:

$$\Delta\theta_1 + \Delta\theta_2 = \Delta\theta_t \tag{27}$$

$$\Delta t_1 + \Delta t_2 = \Delta t_t \tag{28}$$

$$\Delta\theta_1 = \frac{\Delta\theta_{10} C_{b10}}{C_{b1}} \tag{29}$$

$$\Delta\theta_2 = \frac{\Delta\theta_{20} C_{b20}}{C_{b2}} \tag{30}$$

$$\Delta t_1 = \frac{\Delta t_{10} C_{b10}}{C_{b1}} \tag{31}$$

$$\Delta t_2 = \frac{\Delta t_{20} C_{b20}}{C_{b2}} \tag{32}$$

We can now solve analytically for the C_{b1} and C_{b2} required (Eqs. (34) and (37)) to achieve the desired $\Delta\theta_t$ and Δt_t (total change in true anomaly and total time required to reach the terminal point)

$$\Delta\theta_t = \Delta\theta_1 + \Delta\theta_2 = \frac{\Delta\theta_{10}C_{b10}}{C_{b1}} + \frac{\Delta\theta_{20}C_{b20}}{C_{b2}} \tag{33}$$

$$C_{b1} = \frac{\Delta\theta_{10}C_{b10}C_{b2}}{\Delta\theta_t C_{b2} - \Delta\theta_{20}C_{b20}} \tag{34}$$

$$\Delta t_t = \frac{\Delta t_{10}C_{b10}}{C_{b1}} + \frac{\Delta t_{20}C_{b20}}{C_{b2}} \tag{35}$$

$$\Delta t_t = \frac{\Delta t_{10}(C_{b10})(\Delta\theta_t C_{b2} - \Delta\theta_{20}C_{b20})}{\Delta\theta_{10}C_{b10}C_{b2}} + \frac{\Delta t_{20}C_{b20}}{C_{b2}} \tag{36}$$

$$C_{b2} = \frac{C_{b20}(\Delta t_{20}\Delta\theta_{10} - \Delta t_{10}\Delta\theta_{20})}{(\Delta t_t)(\Delta\theta_{10}) - (\Delta t_{10})(\Delta\theta_t)} \tag{37}$$

In this case, $\Delta\theta_t$ will be the same as in the trajectory with t_{swap} calculated for latitude targeting and Δt_t will be the original orbit lifetime plus the desired increase in orbit lifetime necessary for longitude targeting (Δt_d). Note that the time to deorbit and total change in true anomaly of the new trajectory after the terminal point will be the same as for the initial trajectory after this point, so only the drag profile before the terminal point will be manipulated by the targeting algorithm. Because Eqs. (27)-(37) assume that the swap points occur at the same semi major axes for the new and initial trajectories, it will be necessary to update t_{s_new} so that this is the case. This is performed by imposing

$$t_{s_{new}} = \frac{t_{s_{old}}C_{b10}}{C_{b1}} \tag{38}$$

This procedure finds a set of control parameters that will result in minimized latitude and longitude targeting errors. Once the procedure is completed, a new initial trajectory can be configured and propagated with the new t_{swap}, C_{b1}, and C_{b2} values. There may be some error between this newly propagated trajectory and the analytical solution due to the assumptions made in developing the relations used to calculate the analytical solution. However, the newly propagated trajectory will be closer to the ideal trajectory, the analytical solution process can be repeated, and the results can be used to configure and propagate yet another trajectory. This trajectory will have a smaller deviation from the analytical solution. After a few iterations, the analytical solution should agree with the numerical propagation within some tolerance. At this point, the control parameters needed to reduce the latitude and longitude targeting errors below the specified tolerance will be calculated.

IV. Controllability Analysis

Controllability is defined as the ability to achieve any desired final state in a finite amount of time from a given initial state and range of control parameters[19]. If not configured correctly, there may be some cases where the system is unable to target the desired longitude and latitude. This can happen if the maneuver is initiated with insufficient orbit life remaining, if poor C_{b1}, C_{b2}, and t_{swap} values are chosen in the initial trajectory, or if C_{b1} and C_{b2} cannot be varied significantly due to the physical limitations of the spacecraft. This section investigates the factors that contribute to the controllability of the system and investigates the targeting capabilities of the system based on the initial state and available control parameters.

First, let us consider the effects on the impact location of deviations in the value of only t_{swap} from an initial trajectory. Consider the case where t_{swap} is increased while C_{b1} and C_{b2} remain constant. Changing t_{swap} will mean that phase two of the new trajectory (the phase between t_{s_old} and t_{s_new}) will have a different time and change in true anomaly than phase two of the initial trajectory (assuming that C_{b1} and C_{b2} are not identical). The total changes in true anomaly and times required for phases one and three of the new trajectory will be the same as the changes in true anomaly and times required for phases one and three of the initial trajectory as illustrated in Figure 7.

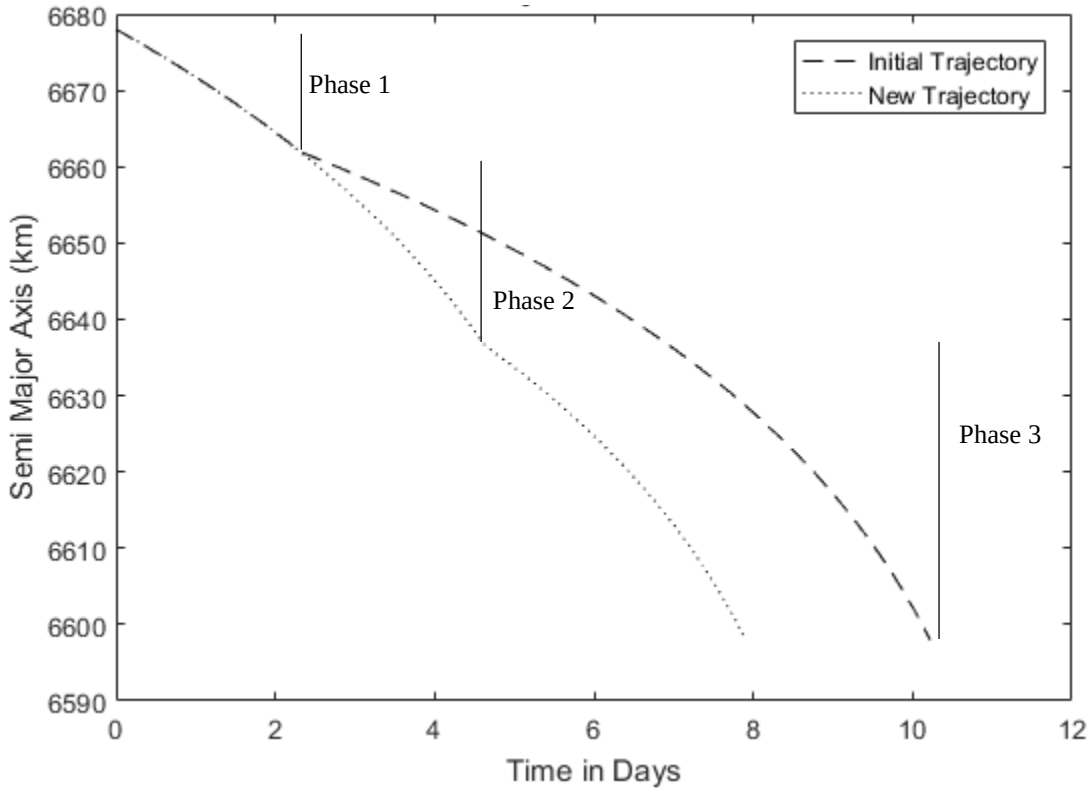

Figure 7. Effects on Trajectory of Only Changing Swap Time

If t_{20} is the time required for phase two of the initial trajectory, the time t_2 required for phase two in the new trajectory is calculated by Eq. (19) as

$$t_2 = \frac{C_{b2} t_{20}}{C_{b1}} \tag{39}$$

This is valid because the initial trajectory has C_{b2} during phase two while the new trajectory has C_{b1} and both trajectories have the same a_0 and a_f during this phase. The total increase in orbit lifetime resulting from the increase in t_{swap} is given by

$$\Delta t_d = t_2 - t_{20} = \Delta t_{swap} - t_{20} \tag{40}$$

Using Eq. (39), Eq. (40) can be rewritten as

$$\Delta t_d = \Delta t_{swap} - \Delta t_{swap}\left(\frac{C_{b1}}{C_{b2}}\right) = \Delta t_{swap}\left(1 - \frac{C_{b1}}{C_{b2}}\right) \tag{41}$$

From this equation, we see that if C_{b1} is greater than C_{b2}, the change in orbit lifetime will be negative given an increase in t_{swap}. This happens because the spacecraft would be spending more time with a higher ballistic coefficient if t_{swap} is increased. The analysis for the case where t_{swap} is decreased is similar, except that the change in t_{swap} is equal to $-t_{20}$ instead of t_2, but Eq. (41) for Δt_d also results. Once the change in orbit lifetime has been calculated, the difference in the total change in true anomaly between the new and old trajectories can be calculated by

$$\Delta\theta_d = \omega_{2\_avg}\Delta t_d \tag{42}$$

Where ω_{2_avg} is the average angular velocity during phase 2 and is calculated based on the initial trajectory. Eq. (42) is valid because all variations in orbit lifetime and changes in true anomaly occur during phase two. Figure 8 and Figure 9 illustrate the increase in orbit lifetime and increase in the total change in true anomaly given a variation in

t_{swap}. The initial conditions were a 300 km circular orbit and the initial t_{swap} was 150,000 seconds (41.67 hours) with ballistic coefficients in units of m^2/kg

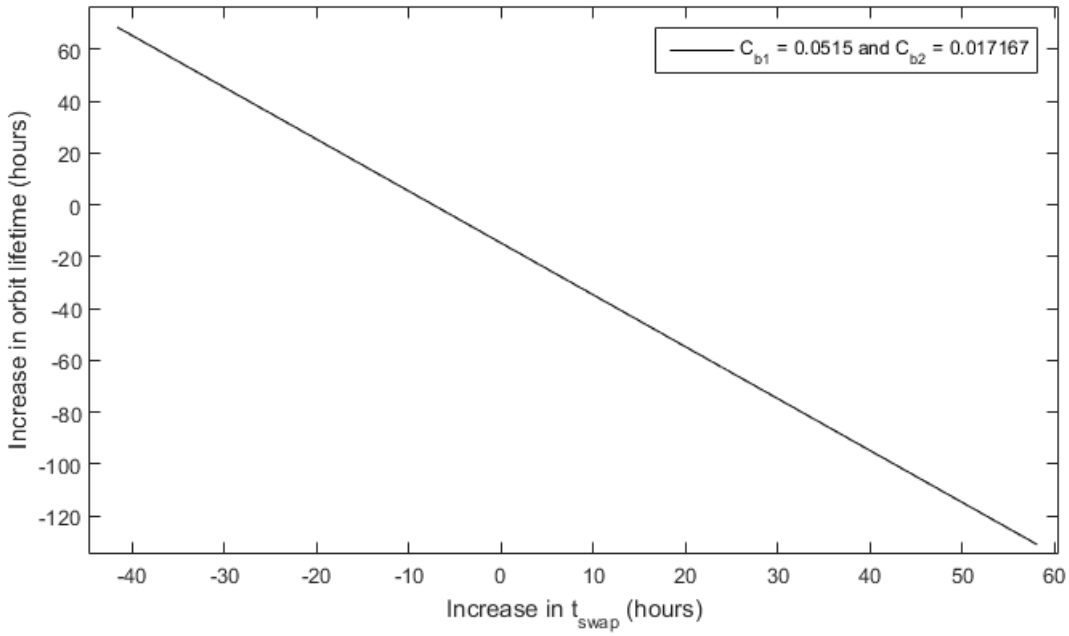

Figure 8. Effects of Changes in Swap Time on Orbit Lifetime

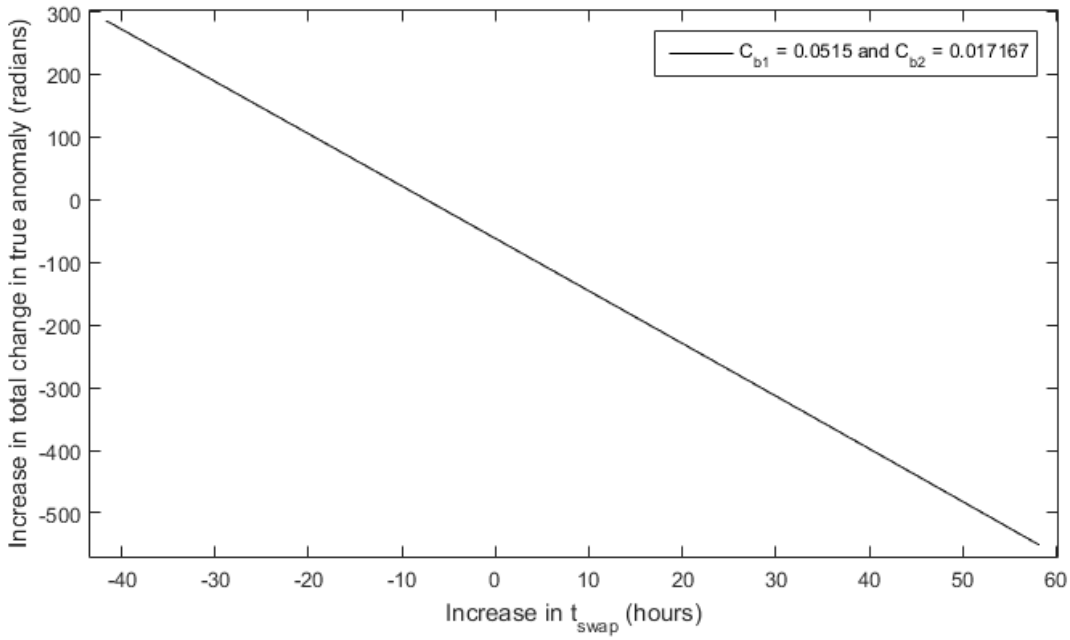

Figure 9. Effects of Changes in Swap Time on Total Change in True Anomaly

The ability to change orbit lifetime by at least 12 hours (43,200 seconds) guarantees that the target longitude will pass beneath the orbital plane at least once and that the longitude error will be no greater than Earth's angle of rotation over half an orbital period. As illustrated by Eq. (41) and Eq. (42), changing t_{swap} will have a greater effect on the total orbit lifetime and change in true anomaly if the ratio of C_{b1} to C_{b2} is greater. Thus, for maximum controllability, it is best to propagate the initial trajectory with the largest ratio of C_{b1} to C_{b2} that the spacecraft is capable of achieving. In the current scenario, because the maximum variation in the total change in true anomaly is well over 2π radians, there will be multiple t_{swap} values that result in zero latitude error as shown in Figure 10 for a 300 km circular orbit with

ballistic coefficients in units of m^2/kg. The high frequency oscillations represent cycles where latitude targeting increases then decreases (eventually passing through zero) while some longitude error remains, and the low frequency oscillations represent increases and decreases in longitude error as the Earth rotates beneath the satellite's orbital plane.

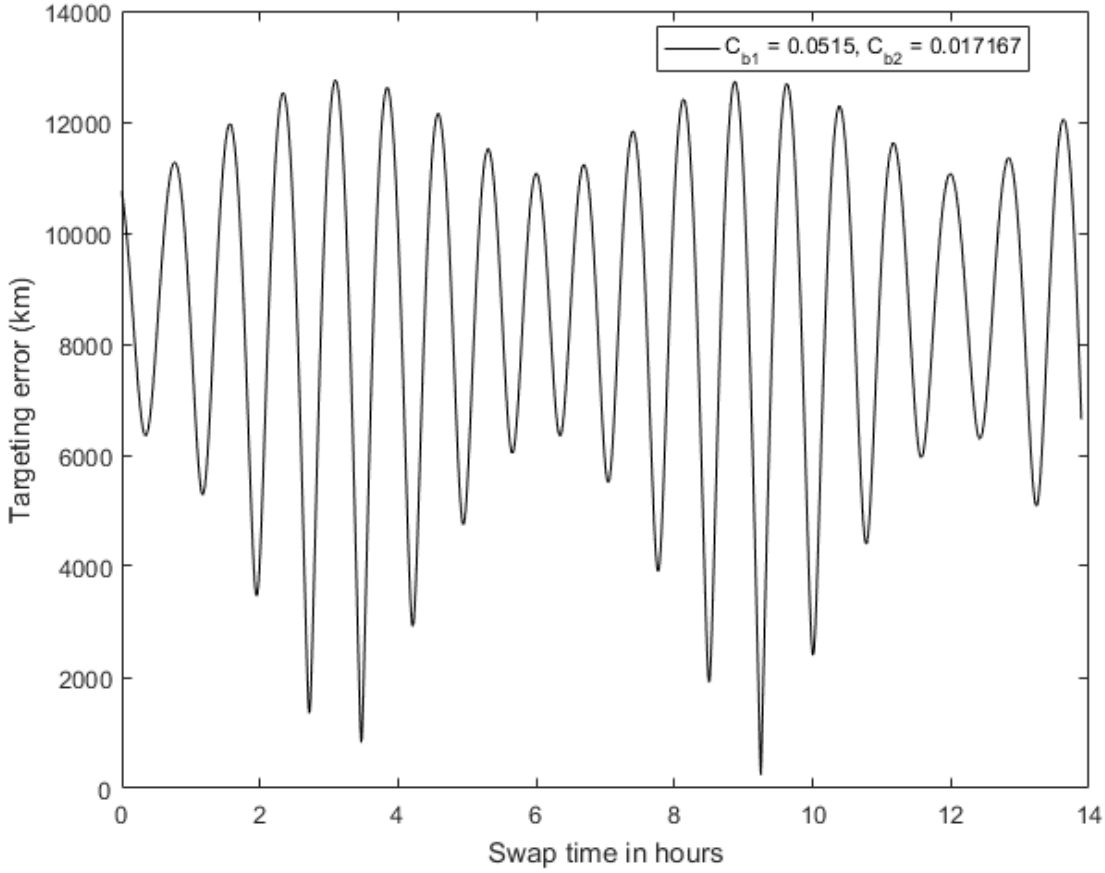

Figure 10. The effects of changes in t_{swap} on total targeting error

From the set of possible swap times, one would want to pick the time that resulted in zero latitude error and the minimum positive longitude error. It is desirable to perform the latitude targeting before the longitude targeting because latitude error is independent of the Earth's rotation while longitude error is not. Fortunately, because there are multiple possible t_{swap} values to choose from, it is likely that longitude error can be made quite small (a few hundred kilometers or less) through only a variation of t_{swap}.

Once the most desirable t_{swap} value has been determined, C_{b1} and C_{b2} must be varied to eliminate the remaining longitude error by changing the orbit lifetime without varying the total change in true anomaly. The maximum amount by which orbit lifetime can be varied will depend on the characteristics of the initial trajectory and the selected t_{swap} value. Recognizing that

$$\Delta\theta_{10} = \omega_{10}\Delta t_{10} \tag{43}$$

$$\Delta\theta_{20} = \omega_{20}\Delta t_{20} \tag{44}$$

$$\Delta\theta_t = \Delta\theta_{10} + \Delta\theta_{20} + \Delta\theta_d \tag{45}$$

$$\Delta t_t = \Delta t_{10} + \Delta t_{20} + \Delta t_d \tag{46}$$

We can rewrite Eq. (37) as

$$C_{b2} = \frac{C_{b20}\left(\Delta t_{20}(\omega_{10} - \omega_{20})\right)}{(\Delta t_{20})(\omega_{10} - \omega_{20}) + (\Delta t_d)\omega_{10} - (\Delta\theta_d)} \tag{47}$$

Assuming $\Delta\theta_d = 0$ (no desired difference in change in true anomaly between the trajectories) and solving for Δt_d yields

$$\Delta t_d = \frac{\Delta t_{20}(\omega_{10} - \omega_{20})}{\omega_{10}}\left(\frac{C_{b20}}{C_{b2}} - 1\right) \tag{48}$$

For a given value of C_{b2}, the C_{b1} needed to ensure $\Delta\theta_d = 0$ is calculated using Eq. (34) and the resulting increase in orbit lifetime (Δt_d) is given by Eq. (48). Because $\omega_{10} < \omega_{20}$ (since ω_{20} applies to a lower orbit), $\omega_{10} - \omega_{20} < 0$. Thus, if $C_{b2} > C_{b20}$, then $\Delta t_d > 0$ and if $C_{b2} < C_{b20}$, then $\Delta t_d < 0$. Therefore, in order to increase Δt_d, C_{b2} should be increased. This will result in a decreased value of C_{b1} required to maintain the same total change in true anomaly. To be able to achieve the maximum possible increase in orbit lifetime, the initial trajectory should be propagated with the lowest possible C_{b2} value and the highest possible C_{b1} value. This will also increase the effect of variations in t_{swap} on the system which will mean that the longitude error will already be small just through changing t_{swap}. The only drawback of a high initial C_{b1} value is that the amount by which orbit lifetime can be decreased will be limited. That is why a positive longitude error is preferable to a negative longitude error. Positive longitude errors mean that the spacecraft has landed East of the target point and are remedied by an increase in orbit lifetime while negative errors are remedied by a decrease in lifetime. Figure 11 illustrates the C_b values required to achieve various increases in total orbit lifetime for a 300 km initial circular orbit with a t_{swap} value of 150,000 seconds (41.67 hours). Note that for certain Δt_d values, the required C_{b1}, and C_{b2} values may not be physically attainable. They may either be out of the performance range of the spacecraft or may even be negative (which is never possible).

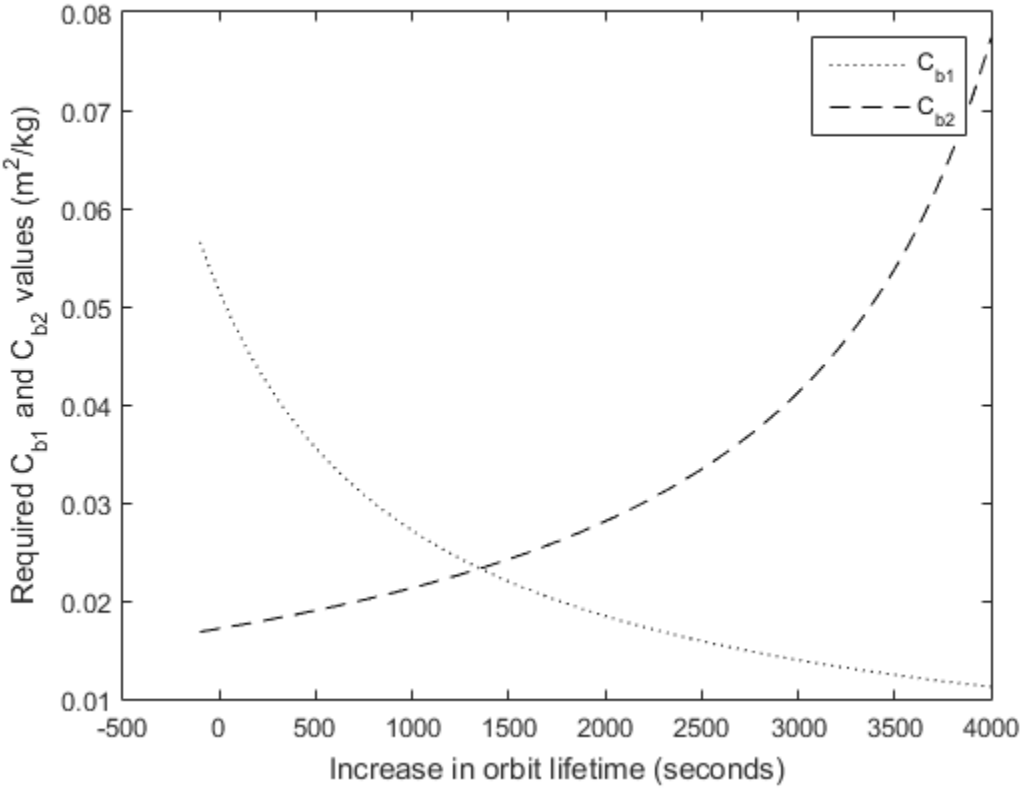

Figure 11. C_b Values Required to Produce Given Changes in Orbit Lifetime (C_{b10} = .0515, C_{b20} = .01717)

To find the maximum Δt_d value, choose the maximum possible C_{b2} value that does not require C_{b1} to be below the minimum value the spacecraft is capable of in order to maintain the same $\Delta\theta_t$. It is also important to note that the chosen value of t_{swap} will have a large effect on the maximum Δt_d. A t_{swap} value that is too close to the beginning or end of the orbit lifetime will result in limited controllability of the total orbit lifetime through variations of C_{b1} and

C_{b2}. Figure 12 shows the maximum Δt_d for various t_{swap} values for a 300 km initial circular orbit with $C_{b10} = .0515$ and $C_{b20} = .01717$ and maximum and minimum C_b values of .1 and .01 m^2/kg respectively.

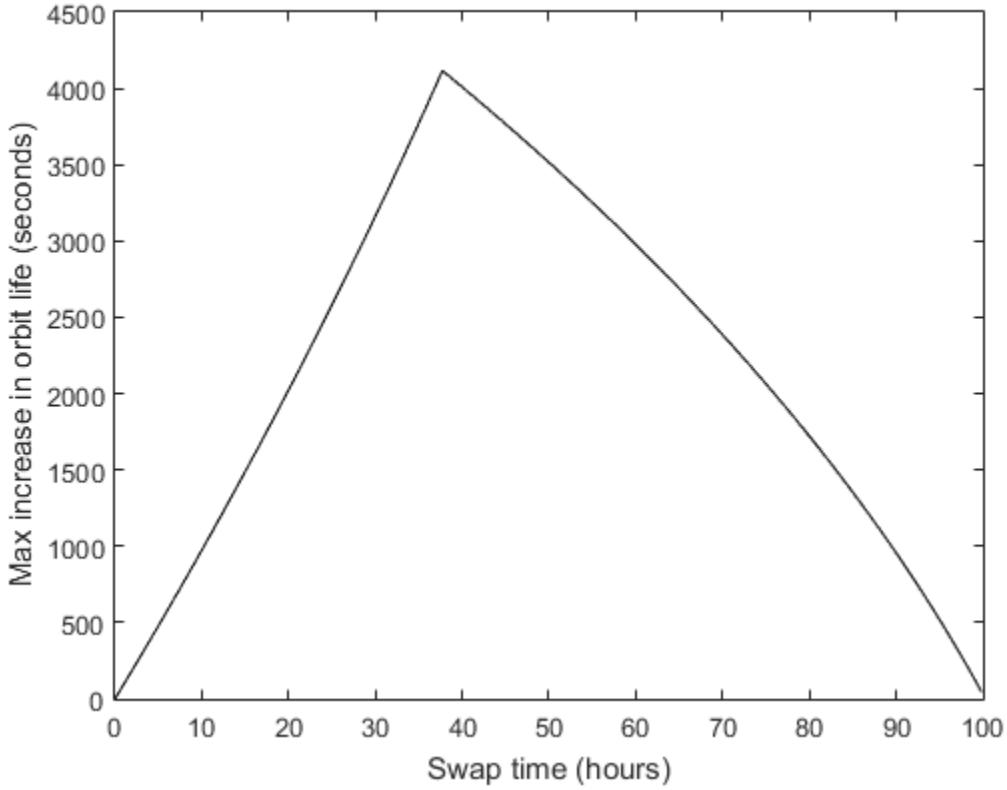

Figure 12. Maximum Possible Change in Orbit Lifetime for Various Swap Times

Ideally, t_{swap} should be chosen as close as possible to the middle of the de-orbit trajectory. In the simulations, a range of t_{swap} values is defined such that the controllability of Δt is reasonable. The t_{swap} within that range that results in zero latitude error and the smallest positive longitude error is then chosen. For this particular set of initial conditions, it is clear to see that there is sufficient controllability to target any desired impact location with a latitude below the orbit inclination.

V. Simulation Results

Simulation results confirmed this targeting capability and demonstrated a targeting error of less than 10 km for all tested desired impact locations with circular initial orbits or mild eccentricities (less than .001). Simulations run times were also low enough to make running this algorithm onboard a small spacecraft feasible. Simulations were conducting using MATLAB R2016a running on an Alienware 13 machine with a 2.4 Ghz Intel i7 Broadwell processor. The ode45 (Runge-Kutta) integrator in MATLAB R2016a was utilized with a tolerance of 1E-11. Beyond the choice of integrator, no additional attempts at optimization were made. In all simulations, C_{b1} and C_{b2} were set to .0515 and .0172 and the target latitude and longitude were (35° N, 10° E). The table below indicates the results of several simulations.

Table 1. Simulation Results

Initial Orbital Elements ($a[km]$, e, $\Omega[deg]$, $\omega[deg]$, $\theta[deg]$, $i[deg]$)	Initial t_{swap} (s)	Atmosphere model	Number Numerically Propagated Trajectories	Orbit Life (hours)	Total targeting error (km)	Simulation Run Time (s)
(6678, 0, 0, 0, 90°, 45°)	100,000	1976 standard	4	248	.95	71
(6678, 0, 0, 0, 90°, 60°)	100,000	1976 standard	4	250	.44	75
(6678, 0, 0, 0, 90°, 90°)	150,000	1976 standard	4	250	.57	76
(6698, 0, 0, 0, 90°, 90°)	150,000	1976 standard	4	310	.03	98
(6678, 0, 90°, 0, 90°, 90°)	150,000	1976 standard	4	256	.56	72
(6678, .001, 0, 0, 90°, 45°)	100,000	1976 standard	10	248	8	161
(6678, .002, 0, 0, 90°, 45°)	100,000	1976 standard	19	246	17	303
(6678, .004, 0, 0, 90°, 45°)	100,000	1976 standard	12	248	48	197
(6678, 0, 0, 0, 90°, 45°)	100,000	NRLMSISE 00	11	176	2.4	1219
(6678, 0, 0, 0, 90°, 90°)	150,000	NRLMSISE 00	13	179	6.2	1728
(6678, .001, 0, 0, 90°, 45°)	100,000	NRLMSISE 00	8	176	8.8	958
(6678, .001, 90°, 0, 90°, 90°)	150,000	NRLMSISE 00	13	185	16	1636

Table 1 shows that the algorithm functioned with less than a one kilometer error for the tested initial conditions with zero eccentricity and converged with an error below 50 km even with an initial eccentricity value of .004 although the equations used to build the algorithm were based on a circular orbit assumption. The targeter converged for eccentric orbits because the effects of the noncircular orbits were captured in the numerically propagated trajectories, and since the analytical solutions were based on these numerically propagated trajectories, the error was minimized. The eccentricity of the international space station can be thought of as an upper bound for the eccentricity of an aerodynamically actuated LEO spacecraft because the impulsive thrusts applied to the space station make its eccentricity far greater than the eccentricity of a satellite under the influence of only aerodynamic drag would be. Small spacecraft launched from the space station will generally have the greatest eccentricity at a given semi major axis. However, aerodynamic drag will cause the eccentricities of these spacecraft to decrease as they deorbit, ensuring that the eccentricities never exceed the initial eccentricity of the space station. This happens because a satellite in an elliptical orbit will experience a greater drag force at the perigee than at the apogee. This will reduce the perigee velocity which will reduce the altitude of the apogee and hence circularize the orbit. Figure 13 shows that the eccentricity of the International Space Station has not exceeded .004 in the past 15 years. Thus, we can assume that the eccentricity of any satellite at the point aerodynamic maneuvering begins will be well below .004 (assuming no impulsive burns) and the targeted de-orbit algorithm will be effective.

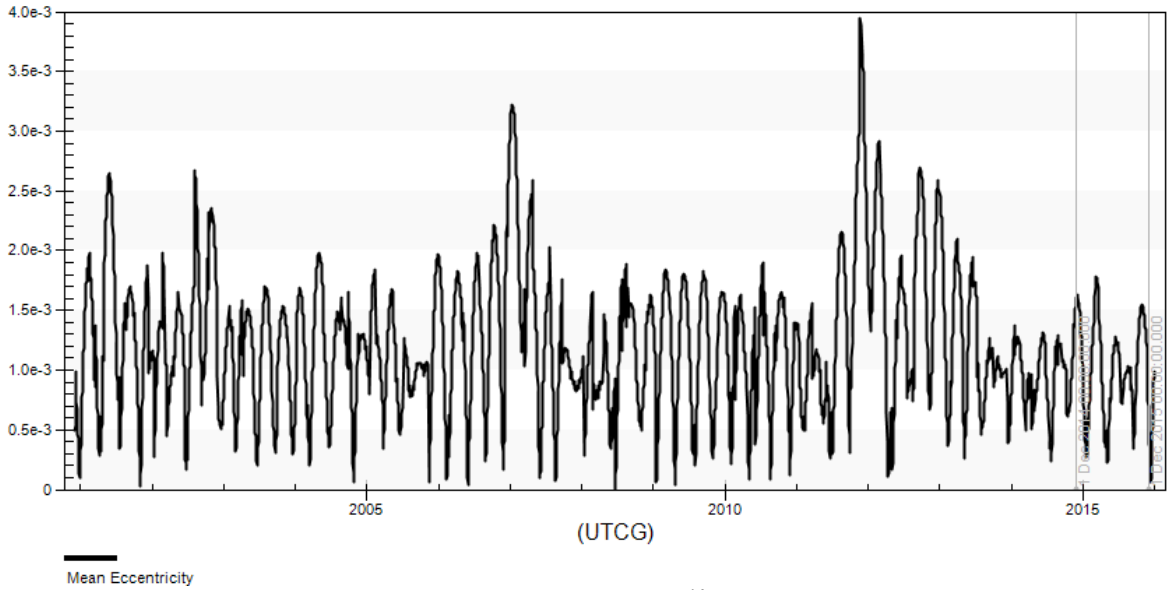

Figure 13. International Space Station Eccentricity over Time[14]

Additionally, Table 1 shows that simulations generally took under five minutes to run even without significant attempts to optimize any of the algorithms. Re-writing the code in C or C++, investigating more efficient integration algorithms, and running the code through a profiler to find areas to reduce computation time could further decrease the required runtime, making this algorithm more feasible to run onboard a satellite. Even if the processor onboard a spacecraft operated at 1/20th the speed of the PC used to run this simulation, the required control parameters and guidance trajectory could be calculated and updated approximately every two hours (assuming the PC would require at most five minutes).

Using a higher fidelity atmospheric model such as the NRLMSISE-00 model results in an increase in the required simulation time and in some cases, the algorithm may fail to converge if unexpected density behavior occurs. In such a case, the NRLMSISE-00 model can be utilized to create a profile of average density vs. altitude in the regions where the spacecraft is expected to fly, and this density profile can be used instead of the standard atmospheric density model. Because the density at any given altitude will be constant, the performance and convergence properties of the algorithm will be the same as when the 1976 standard atmosphere is used.

VI. Conclusions

Through simulations and mathematical analysis, the feasibility of targeting an impact location with a spacecraft using solely aerodynamic drag has been demonstrated. Numerically propagating a single trajectory with an initial ballistic coefficient, second ballistic coefficient, and final ballistic coefficient and defined transition points between the ballistic coefficients provided a reference from which the impact points of trajectories with the same initial conditions but different ballistic coefficient profiles could be calculated analytically. As long as deviations between the initial numerically propagated trajectory and the new trajectories were small, the analytical solutions provided reasonable estimates of the impact locations for the new trajectories. Using the analytical solutions, the rapid calculation of the trajectory control parameters (first and second ballistic coefficients and swap time) necessary to target a desired impact latitude and longitude was possible. This was done by decoupling the latitude and longitude targeting. The swap time was varied first to ensure optimal latitude targeting while achieving the minimum positive longitude error. Calculation of the swap time was treated as an optimization problem of one variable and was performed by analytically calculating the impact location for numerous different t_{swap} values, finding two t_{swap} values that served as upper and lower bounds for the ideal t_{swap}, and then using the bisection method to find the ideal t_{swap} between these two values. After this, the increase in orbit lifetime required for the Earth to rotate into the proper position for longitude targeting was calculated. The first and second ballistic coefficients necessary to achieve this change in orbit lifetime without upsetting the latitude targeting were then calculated analytically. Once these control parameters were calculated, a new trajectory was created with the spacecraft initial conditions and was numerically propagated with the new control parameters. The algorithm was repeated using this new trajectory in place of the initial numerical trajectory. Because the impact location of the new numerically propagated trajectory was closer to the desired impact location, the discrepancy between the analytically calculated impact location of the next trajectory

and the impact location obtained by numerically propagating that new trajectory was smaller than in the first iteration. After each iteration, the difference between the analytical and numerical solutions became smaller and smaller until convergence was achieved and the ballistic coefficient profile needed for impact point targeting was determined.

The targeting algorithm was tested with eccentric initial conditions and nonstandard density values using the NRLMSISE model. In both cases, the algorithm converged and provided the optimal control parameters required for impact point targeting. With the NRLMSISE model, propagating trajectories took longer, and the algorithm took longer to converge. This was because the assumption that density was a function of only altitude no longer held, and variations in the control parameters caused the analytical and numerical solutions to diverge more rapidly than with the standard atmospheric density model. With the nonstandard density model, there were some edge cases that resulted in the failure of the algorithm to converge.

Overall, the algorithm performed very well in calculating the optimal control parameters for impact point targeting. In practice, the numerically propagated trajectory using these parameters would be used to create a guidance for the spacecraft to follow. The drag device would then continuously deploy or retract as needed to ensure that the spacecraft followed the desired trajectory.

VII. Future Work

As of now, the backbone of the impact point targeting algorithm has been created. The simulation framework shall be updated to ensure that there are no edge cases that cause errors.

The simulator will also be upgraded to incorporate J2, solar gravity, and lunar gravity effects and the guidance generation algorithm will be improved so that nonstandard atmospheric density is handled more effectively. The addition of J2 effects will also require the use of mean orbital elements (instead of osculating elements). The effectiveness of the current control algorithm will be analyzed in the face of uncertain environmental perturbations. Since algorithm relies on analyzing perturbations from an initial numerically propagated trajectory, and the effects of nonstandard density and orbital perturbations are taken into account in the initial trajectory, the analytical solution is expected to retain a reasonable level of accuracy even with environmental perturbations. For this reason, the control algorithm is expected to still function properly with higher fidelity environmental models, but convergence times may be slightly longer. AGI's Systems Toolkit will be utilized to test the algorithm with a higher fidelity orbit propagator.

Perhaps the greatest amount of remaining work is in the development of the inner loop guidance tracking algorithm needed to ensure that the spacecraft actually follows the desired decay trajectory. The targeting algorithm discussed in this paper provides the C_{b1}, C_{b2}, and t_{swap} values required to impact the earth in the desired location, but these values are based on a model containing numerous uncertainties, especially in the atmospheric density and drag coefficient. These uncertainties will mean that the satellite will not end up in the desired location if the ballistic coefficient control is applied open loop. In addition, because this algorithm involves several days' worth of orbits, any small initial errors or uncertainties will result in very large errors by the time the spacecraft de-orbits. For these reasons, open loop control of the ballistic coefficient will be insufficient and a feedback control loop will be necessary to ensure that the spacecraft tracks the trajectory specified by the targeting algorithm. Once the ideal control parameters have been calculated by the targeting algorithm, a guidance trajectory will be created consisting of specified values of orbital elements at each point in time during the desired decay trajectory. Because the uncertain orbital perturbations (such as aerodynamic drag) primarily affect in-plane motion, the orbital parameters that will experience the most error are true anomaly and semi major axis. Since semi major axis is related to mean motion (the average rate of change of true anomaly), knowledge of the desired and actual true anomaly and rate of change of true anomaly is sufficient to characterize the in-plane error in the system. Based on the discrepancy between the desired and actual true anomaly and rate of change of true anomaly, a control algorithm can be designed to calculate how much the drag device should be deployed or retracted to help return the spacecraft to the guidance trajectory. Adaptive control methods will be utilized for this because the controller tuning will depend heavily on ambient density which is a widely varying parameter.

Once the targeting algorithm and inner loop guidance tracking algorithm are complete, validation via Monte Carlo simulations will be necessary prior to actual deployment of the algorithms on a spacecraft. These simulations will test the algorithms under a variety of different initial conditions with a variety of different system properties (such as minimum and maximum C_b). These simulations will provide information about how well the algorithms work, when they are effective, and when they cease to be effective. The STK orbit propagator will be utilized in the simulations to further verify the effectiveness of the control algorithms under a variety of perturbations including solar gravity, lunar gravity, solar pressure, and the non-uniform gravitational field of Earth. Once the algorithms have been verified and proven to be effective and robust under a variety of reasonable conditions, it will be time to deploy the targeting and guidance tracking algorithms on a real spacecraft and attempt to target a re-entry point.

Acknowledgements

The authors wish to thank AI Solutions for sponsoring this investigation under a NASA Kennedy Space Center's subcontract (project *LSP 15-025: A Drag Device for Controlled Deorbiting of LEO Spacecraft*). The authors also wish to thank Justin Treptow and Larry Fineberg from NASA, Scott Clark and Yusef Johnson from AI Solutions, and Dr. David C. Guglielmo from the University of Florida ADAMUS lab for their revision work and valuable suggestions.

VIII. References

[1] Patera, R. P., and Ailor, W. H., "The realities of reentry disposal," *Proceedings of the AAS/AIAA Space Flight Mechanics Meeting*, 1998, pp. 9–11.

[2] Ailor, W. H., and Patera, R. P., "Spacecraft re-entry strategies: Meeting debris mitigation and ground safety requirements," *Proceedings of the Institution of Mechanical Engineers, Part G: Journal of Aerospace Engineering*, vol. 221, Jun. 2007, pp. 947–953.

[3] Heiney:KSC, A., "NASA - Landing 101" Available: http://www.nasa.gov/mission_pages/shuttle/launch/landing101.html.

[4] National Aeronautics and Space Administration, "Guidance and Navigation for Entry Vehicles," 1968.

[5] Moore, T. E., *Space shuttle entry terminal area energy management*, 1991.

[6] Heidt, H., Puig-Suari, J., Moore, A., Nakasuka, S., and Twiggs, R., "CubeSat: A New Generation of Picosatellite for Education and Industry Low-Cost Space Experimentation," *AIAA/USU Conference on Small Satellites*, Aug. 2000.

[7] Skrobot, G. L., and Coelho, R., "ELaNa-Educational Launch of Nanosatellite Providing Routine RideShare Opportunities," 2012.

[8] Moe, K., and Moe, M. M., "Gas–surface interactions and satellite drag coefficients," *Planetary and Space Science*, vol. 53, Jul. 2005, pp. 793–801.

[9] Pérez, D., and Bevilacqua, R., "Neural Network based calibration of atmospheric density models," *Acta Astronautica*, vol. 110, May 2015, pp. 58–76.

[10] Omar, S. R., and Wersinger, J. M., "Satellite Formation Control using Differential Drag," *53rd AIAA Aerospace Sciences Meeting*, American Institute of Aeronautics and Astronautics, .

[11] Pérez, D., and Bevilacqua, R., "Differential Drag-Based Reference Trajectories for Spacecraft Relative Maneuvering Using Density Forecast," *Journal of Spacecraft and Rockets*, vol. 53, Jan. 2016, pp. 234–239.

[12] Pastorelli, M., Bevilacqua, R., and Pastorelli, S., "Differential-drag-based roto-translational control for propellant-less spacecraft," *Acta Astronautica*, vol. 114, Sep. 2015, pp. 6–21.

[13] Josep Virgili, P. C. E. R., "Atmospheric Interface Reentry Point Targeting Using Aerodynamic Drag Control," *Journal of Guidance, Control, and Dynamics*, vol. 38, 2015, pp. 1–11.

[14] Analytical Graphics Inc, *Systems Toolkit*.

[15] Guglielmo, D., and Bevilacqua, R., "Propellant-less Atmospheric Differential Drag LEo Spacecraft (PADDLES) Mission," *SmallSat Conference*, 2014.

[16] Mason, C., Tilton, G., Vazirani, N., Spinazola, J., Guglielmo, D., Robinson, S., Bevilacqua, R., and Samuel, J., "Origami-based Drag Sail for CubeSat Propellant-free Maneuvering," Tokyo, Japan: 2013.

[17] Vallado, D., *Fundamentals of Astrodynamics and Applications*, Microcosm Press, .

[18] International Organization for Standardization, "ISO/DIS 14222, Space Environment (natural and artificial) - Earth Upper Atmosphere," Sep. 2013.

[19] Franklin, G., Powell, J., and Emami-Naeini, A., *Feedback Control of Dynamic Systems*, Prentice Hall, 2002.